

# Journal Pre-proof

Less is better: Insight into the concentration dependency of the photoreduction of  $\text{Eu}^{3+}$  in  $\text{Ba}_2\text{SiO}_4$

Zetian Yang, Jieqi Hu, David Van der Heggen, Mengmeng Jiao, Henk Vrielinck, Philippe F. Smet, Dirk Poelman

PII: S0022-2313(23)00372-1

DOI: <https://doi.org/10.1016/j.jlumin.2023.120039>

Reference: LUMIN 120039

To appear in: *Journal of Luminescence*

Received Date: 25 May 2023

Revised Date: 20 June 2023

Accepted Date: 28 June 2023

Please cite this article as: Z. Yang, J. Hu, D. Van der Heggen, M. Jiao, H. Vrielinck, P.F. Smet, D. Poelman, Less is better: Insight into the concentration dependency of the photoreduction of  $\text{Eu}^{3+}$  in  $\text{Ba}_2\text{SiO}_4$ , *Journal of Luminescence* (2023), doi: <https://doi.org/10.1016/j.jlumin.2023.120039>.

This is a PDF file of an article that has undergone enhancements after acceptance, such as the addition of a cover page and metadata, and formatting for readability, but it is not yet the definitive version of record. This version will undergo additional copyediting, typesetting and review before it is published in its final form, but we are providing this version to give early visibility of the article. Please note that, during the production process, errors may be discovered which could affect the content, and all legal disclaimers that apply to the journal pertain.

© 2023 Published by Elsevier B.V.



**Less is better: Insight into the concentration dependency of the photoreduction of  $\text{Eu}^{3+}$  in  $\text{Ba}_2\text{SiO}_4$**

Zetian Yang<sup>a</sup>, Jieqi Hu<sup>a</sup>, David Van der Heggen<sup>a</sup>, Mengmeng Jiao<sup>b</sup>, Henk Vrielinck<sup>c</sup>, Philippe F. Smet<sup>a</sup>, and Dirk Poelman<sup>a\*</sup>

<sup>a</sup>LumiLab, Department of Solid State Sciences, Ghent University, Krijgslaan 281-S1, Ghent B-9000, Belgium

<sup>b</sup>College of Physics and Optoelectronic Engineering, Ludong University, Yantai 264025, China

<sup>c</sup>Electron Magnetic Resonance Group, Department of Solid State Sciences, Ghent University, Krijgslaan 281-S1, Ghent B-9000, Belgium

Correspondence:

Prof. Dirk Poelman: E-mail address: [dirk.poelman@ugent.be](mailto:dirk.poelman@ugent.be); Full postal address: LumiLab, Department of Solid State Sciences, Ghent University, Krijgslaan 281-S1, Ghent B-9000, Belgium.

**Abstract**

Photoinduced electron transfer processes in luminescent materials drive numerous applications like medical imaging, ionizing radiation dosimetry and safety signage. However, the concentration dependency of the photoreduction of the dopants during this process is still poorly understood. Here, optical spectroscopy and electron paramagnetic resonance (EPR) experiments are systematically performed to reveal the doping concentration-dependent photoreduction behavior in  $\text{Ba}_{2-x}\text{Eu}_x\text{SiO}_4$  where a fraction of the  $\text{Eu}^{3+}$  dopants can be reduced to  $\text{Eu}^{2+}$  upon irradiation with X-rays. EPR measurements show that the conversion ratio of  $\text{Eu}^{3+} \rightarrow \text{Eu}^{2+}$  decreases with increasing concentration at the same irradiation dose, resulting in the concentration dependency of the photoreduction behavior in  $\text{Ba}_{2-x}\text{Eu}_x\text{SiO}_4$ . Optical spectroscopy measurements show that although the incorporated  $\text{Eu}^{3+}$  ions occupy at least three crystallographic sites,  $\text{Eu}^{3+}$  can only be photoreduced on one of these sites. Meanwhile, the relative occupancy of this photoreducible site decreases as the doping concentration increases. The combination of these two factors might be responsible for the decreased conversion ratio of  $\text{Eu}^{3+} \rightarrow \text{Eu}^{2+}$  as the doping concentration increases. These findings provide insights into the photoreduction of dopants in luminescent materials and can facilitate the exploration of this functional behavior for advanced devices.

**Keywords:** luminescent materials, photo-induced charge transfer,  $\text{Ba}_{2-x}\text{Eu}_x\text{SiO}_4$ , radiation dosimetry

## 1. Introduction

Luminescent materials or phosphors are generally considered to be materials that can emit light upon exposure to some sort of excitation such as ionizing radiation or UV light.<sup>1</sup> In inorganic phosphors the luminescence is often the result of a localized electronic transition of a dopant ion or crystallographic defect that was incorporated in the material, either intentionally or by accident.<sup>2</sup> Some of these defects can also act as charge trapping centers sometimes enabling photoinduced charge transfer process between defects which can give rise to technologically interesting behavior such as afterglow<sup>2,4</sup>, optically stimulated luminescence<sup>5,6</sup> or photochromism<sup>7-9</sup>.

Naturally this photoinduced charge transfer process results in a reversible oxidation or reduction of the involved defects.<sup>10-13</sup> In  $\text{Sr}_4\text{Al}_{14}\text{O}_{25}:\text{Eu},\text{Dy}$  for example an electron is transferred from Eu to Dy upon exposure to blue or UV light or X-rays.<sup>13</sup> But this was also observed in  $\text{Ba}_{2-x}\text{Eu}_x\text{SiO}_4$  where the  $\text{Eu}^{3+}$  can be reduced upon exposure to X-rays, resulting in a pronounced change in the photoluminescence color from red ( $\text{Eu}^{3+}$ ) to green ( $\text{Eu}^{2+}$ ).<sup>14,15</sup>

The number of trapped charges during exposure is usually proportional to the deposited dose in a certain range. Provided that the trapped charges are stable under the measurement and storage conditions and that information on the amount of trapped charges can be obtained through, e.g. optically stimulated luminescence or a luminescence intensity ratio, it is possible to use these materials for radiation dosimetry after proper calibration.<sup>16,17</sup> Inspired by this, various luminescent materials with photoinduced valence change behavior have been developed for dosimetry applications based on different hosts or different dopants<sup>17</sup> like Ag-doped sodium aluminophosphate glass<sup>18,19</sup>,  $\text{Al}_2\text{O}_3:\text{C},\text{Mg}^{20}$ ,  $\text{Ba}_2\text{SiO}_4:\text{Eu}$ ,<sup>14,15</sup>  $\text{KSrPO}_4:\text{Eu}^{21}$ ,  $\text{NaCl}:\text{Yb}^{22}$ ,  $\text{CaF}_2:\text{Sm}^{23}$  and  $\text{CaSO}_4:\text{Sm}^{24}$ .

For the abovementioned lanthanide-doped compounds, in particular those doped with  $\text{Eu}^{3+}$  or  $\text{Sm}^{3+}$ , a fraction of the dopants are reduced to a divalent state upon irradiation with UV light or X-rays.<sup>14,22,25-28</sup> The hole-trapping defects that act as the redox-partner are often not identified although in some cases their optical properties could be characterized. For some of these materials it was found that a higher conversion ratio (i.e. a higher degree of photoreduction of the trivalent dopant) is achieved at a lower doping concentration.<sup>21,28-31</sup> Such an unusual behavior is usually ascribed to the partial luminescence quenching of the

photoreduced dopant by surrounding defects or to the limited availability of the involved hole trapping defects in the host during photoreduction processes. In general, however, the underlying mechanisms are still poorly understood.

In this work, we investigated the doping concentration dependency of the photoreduction processes in  $\text{Ba}_{2-x}\text{Eu}_x\text{SiO}_4$  ( $x = 0.001, 0.005, 0.02, 0.04$ ) which shows a valence change of  $\text{Eu}^{3+} \rightarrow \text{Eu}^{2+}$  upon irradiation.<sup>14,15</sup> Electron paramagnetic resonance (EPR) measurements show that the conversion ratio of  $\text{Eu}^{3+} \rightarrow \text{Eu}^{2+}$  decreases with the increase in concentration at the same irradiation dose, resulting in the concentration dependency of the photoreduction behavior in  $\text{Ba}_{2-x}\text{Eu}_x\text{SiO}_4$ . The decreased conversion ratio might be caused by the occupancy site-dependent photoreduction behavior of  $\text{Eu}^{3+}$  and the concentration-dependent site occupancy of  $\text{Eu}^{3+}$ . The insight into this behavior is expected to provide guidelines for the development of high-performance dosimeters.

## 2. Experimental section

*Sample preparation:*  $\text{Ba}_{2-x}\text{Eu}_x\text{SiO}_4$  ( $x = 0.001, 0.005, 0.02, 0.04$  and  $0.06$ ) samples were synthesized using a solid-state reaction.  $\text{BaCO}_3$  (Alfa Aesar, 99.8%),  $\text{SiO}_2$  (Alfa Aesar, 99.5%), and  $\text{Eu}_2\text{O}_3$  (Alfa Aesar, 99.99%) were used as raw materials without further purification and weighed according to the chemical formula. 10 mol% of  $\text{H}_3\text{BO}_3$  was added as the sintering aid. The powders were ball-milled with ethanol for 5 h at a rotating speed of 300 rpm followed by drying in an oven at 60 °C. Then, the powders were mixed with a polyvinyl alcohol (5 wt%) and pressed into pellets. The pellets were sintered at 1200 °C for 5 h under different conditions (90%  $\text{N}_2$ + 10%  $\text{H}_2$ , or air) to get dense ceramics.

*Sample characterization:* Phase structures of synthesized samples were confirmed by powder X-ray diffraction (XRD) using a Siemens D5000 diffractometer (40 kV, 40 mA) with  $\text{Cu K}\alpha$  radiation ( $\lambda = 0.154$  nm). Room-temperature photoluminescence emission (PL) and excitation (PLE) spectra were measured using an Edinburgh FS920 (Edinburgh Instruments Ltd, Livingston, UK) fluorescence spectrometer. In situ PL spectra after X-ray irradiation with different doses were measured with a home-built setup and using an Ocean Optics QE65000 array spectrometer under the excitation of a 365 nm LED (FWHM = 16 nm).<sup>14</sup> The X-ray irradiation experiments were performed using a Siemens D5000 X-ray diffractometer (Cu anode, not filtered) operated at 40 kV, 10 mA, yielding an estimated air kerma rate of 3.75 Gy

$\text{min}^{-1}$  at the position of the sample. An NT340 series tunable OPO laser (EKSPLA, Lithuania), was employed to perform the reduction processes upon 270 nm irradiation. The reflectivity was measured using a PerkinElmer Lambda1050 UV-vis-NIR spectrophotometer equipped with a Spectralon-coated integrating sphere with PMT (photomultiplier) and InGaAs detectors. Decay times were collected using an EKSPLA NT340 series tunable laser as an excitation source in combination with an Andor intensified CCD. The decay process of  $\text{Eu}^{2+}$  was measured by monitoring the range of 450 - 570 nm. The decay process of  $\text{Eu}^{3+}$  in site A, site B and site C was measured by monitoring the range of 571 - 573.5 nm, 577 - 578.5 nm, and 578.5 - 580 nm respectively. Electron paramagnetic resonance (EPR) measurements were performed on a Bruker ElexSys E500 spectrometer operating at Q-band (34 GHz) and room temperature. For the same composition sintered under different atmosphere conditions, the same amount of powder was measured using the same size tube to ensure that the signal intensity of the same sample synthesized in different atmosphere conditions were comparable.

### 3. Results and discussion

A comparison of the obtained XRD patterns (Figure 1a) to the reference cards of PDF#26-1403 ( $\text{Ba}_2\text{SiO}_4$ ) indicates that a pure orthorhombic structure with space group of  $Pnma$  is formed in all  $\text{Ba}_{2-x}\text{Eu}_x\text{SiO}_4$  ( $x=0.001, 0.005, 0.02, 0.04, \text{ and } 0.06$ ) powders. In  $\text{Ba}_2\text{SiO}_4$ ,  $\text{Ba}^{2+}$  occupies two inequivalent sites with a ten- and a nine-fold oxygen coordination of  $C_s$  symmetry (Figure 1b).<sup>32</sup> The PL spectra of  $\text{Ba}_{2-x}\text{Eu}_x\text{SiO}_4$  sintered in air and  $\text{N}_2+\text{H}_2$  are shown in Figure 1c and 1d, respectively. For the samples sintered in air, only the typical intraconfigurational  $4f^6$  ( ${}^5D_0 \rightarrow {}^7F_J$  ( $J = 0, 1, 2, 3, 4$ )) transitions of  $\text{Eu}^{3+}$  are observed. For the PL spectra of  $\text{Eu}^{3+}$ , the  ${}^5D_0 \rightarrow {}^7F_1$  transition directly reflects the crystal-field splitting of the  ${}^7F_1$  level and the splitting situation of the  ${}^7F_1$  level is affected by symmetry of the site occupied by  $\text{Eu}^{3+}$ .<sup>33</sup> As the doping concentration increases, the shape change of the  ${}^5D_0 \rightarrow {}^7F_1$  transition indicates that the occupancy situation of  $\text{Eu}^{3+}$  at crystallographic sites changes. When the samples are sintered in  $\text{N}_2+\text{H}_2$ , only the  $4f^6 5d^1 \rightarrow 4f^7$  transition of  $\text{Eu}^{2+}$  appears.<sup>34</sup> With increasing doping concentration, the slight redshift of the emission peak of  $\text{Eu}^{2+}$  might be caused by the re-absorption of emitted light. Furthermore, the PL intensity increases with concentration up to  $x = 0.04$  and  $x = 0.02$  for the samples sintered in air and  $\text{N}_2+\text{H}_2$ , respectively. At higher concentrations the luminescence of the sample decreases due to the concentration quenching

(Figure 1e).<sup>35,36</sup> As reported in previous research, a fraction of  $\text{Eu}^{3+}$  can be converted into  $\text{Eu}^{2+}$  upon irradiation with X-rays if the sample is first sintered in air.<sup>14,15</sup> This is also observed in this work (Figure 1f), where an additional emission band related to the  $4f^65d^1 \rightarrow 4f^7$  transition of  $\text{Eu}^{2+}$  appears after X-ray irradiation. For the photoreduction upon X-ray irradiation, this process is likely the creation of electron-hole pairs, followed by the electron being trapped at  $\text{Eu}^{3+}$  to form  $\text{Eu}^{2+}$ , while the hole is presumably trapped at redox-partner defects.<sup>14,37</sup> In addition, a reversible valence change of  $\text{Eu}^{3+} \leftrightarrow \text{Eu}^{2+}$  can be induced upon appropriately alternating UV/visible light stimuli (Figure S1). Similar behavior has been systematically investigated in certain lanthanides doped barium phosphate.<sup>38</sup> The dose dependency of the photoreduction can be exploited for radiation dosimetry, where the incident dose is encoded into the photoluminescence intensities of Eu in its different valence states.

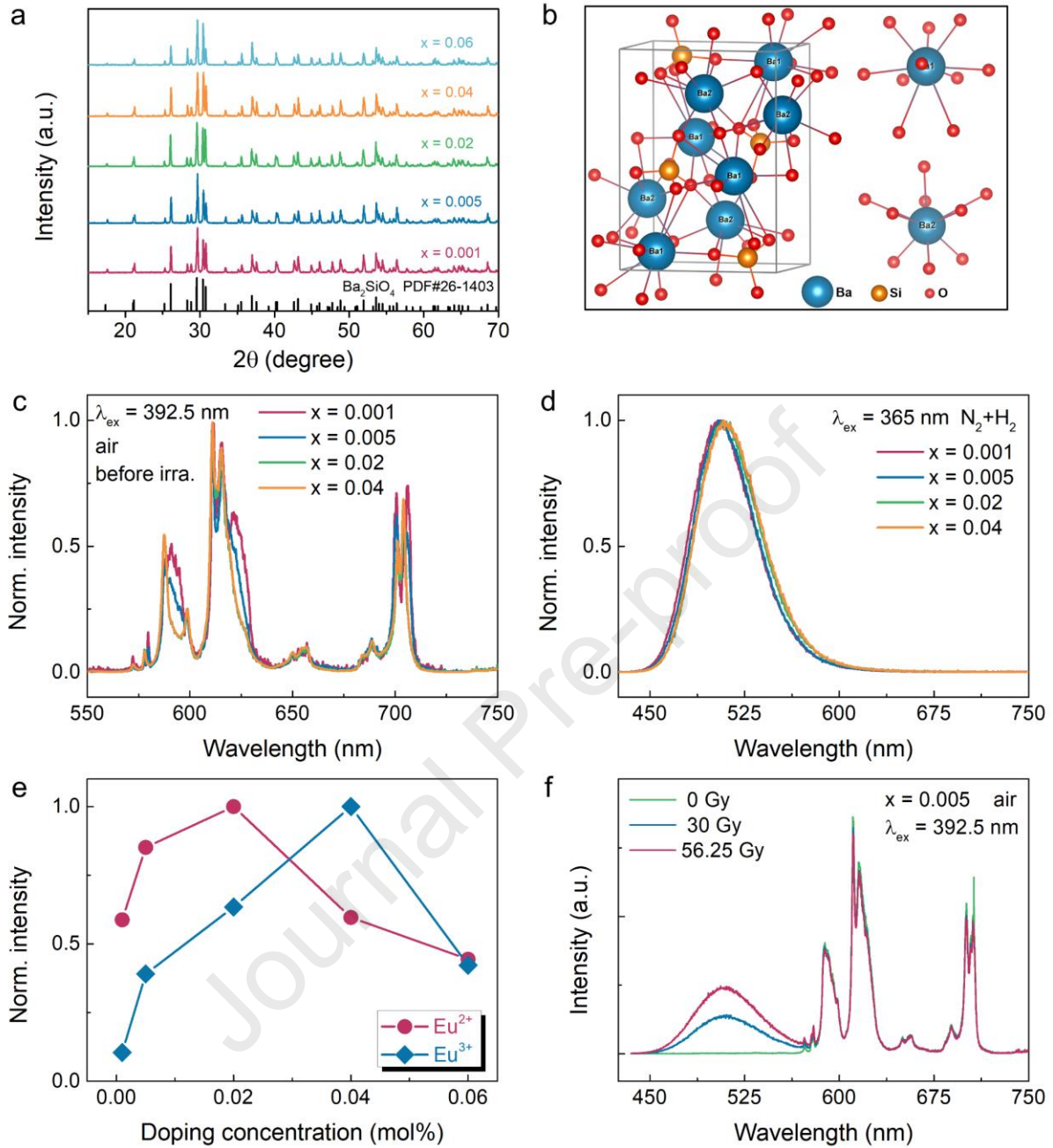


**Figure 1.** (a) XRD patterns of  $\text{Ba}_{2-x}\text{Eu}_x\text{SiO}_4$ . (b) Crystal structure of  $\text{Ba}_2\text{SiO}_4$ . (c) PL spectra ( $\lambda_{\text{ex}} = 392.5$  nm) of  $\text{Ba}_{2-x}\text{Eu}_x\text{SiO}_4$  sintered in air. (d) PL spectra ( $\lambda_{\text{ex}} = 365$  nm) of  $\text{Ba}_{2-x}\text{Eu}_x\text{SiO}_4$  sintered in  $\text{N}_2+\text{H}_2$ . (e) Doping concentration dependency of PL intensities of  $\text{Eu}^{2+}$  (sintered in  $\text{N}_2+\text{H}_2$ ,  $\lambda_{\text{ex}} = 365$  nm) and  $\text{Eu}^{3+}$  (sintered in air,  $\lambda_{\text{ex}} = 392.5$  nm). (f) PL spectra ( $\lambda_{\text{ex}} = 392.5$  nm) of  $\text{Ba}_{1.995}\text{Eu}_{0.005}\text{SiO}_4$  sintered in air after irradiation with different doses.

To determine the optimal concentration for dosimetry, the dose dependency of photoreduction behavior in  $\text{Ba}_{2-x}\text{Eu}_x\text{SiO}_4$  is investigated (Figures 2a-2d). When the irradiation dose increases,

the emission intensity of  $\text{Eu}^{2+}$  gradually increases for all samples. This change is accompanied by a decrease in the emission intensity of  $\text{Eu}^{3+}$ . Here, one should note that the difference between the PL spectra in Figure 2b and Figure 1f is due to the different excitation wavelengths. The dose dependency of  $I_{\text{Eu}^{2+}}$  and  $I_{\text{Eu}^{2+}}/I_{\text{Eu}^{3+}}$  are presented in Figures 2e and 2f, respectively, where  $I_{\text{Eu}^{2+}}$  and  $I_{\text{Eu}^{3+}}$  are integrated over the range of 450-560 nm and 675-725 nm, respectively. The intensity ratio has previously been identified as a useful and self-calibrated quantity to obtain information about the radiation dose.<sup>14</sup> The results show that the photoreduction behavior of  $\text{Eu}^{3+}$  depends on the doping concentration. While  $I_{\text{Eu}^{2+}}$  increases with doping concentration,  $I_{\text{Eu}^{2+}}/I_{\text{Eu}^{3+}}$  decreases. This indicates that a higher response can be obtained at a lower doping concentration if the self-calibrated  $I_{\text{Eu}^{2+}}/I_{\text{Eu}^{3+}}$  is selected as the response parameter.

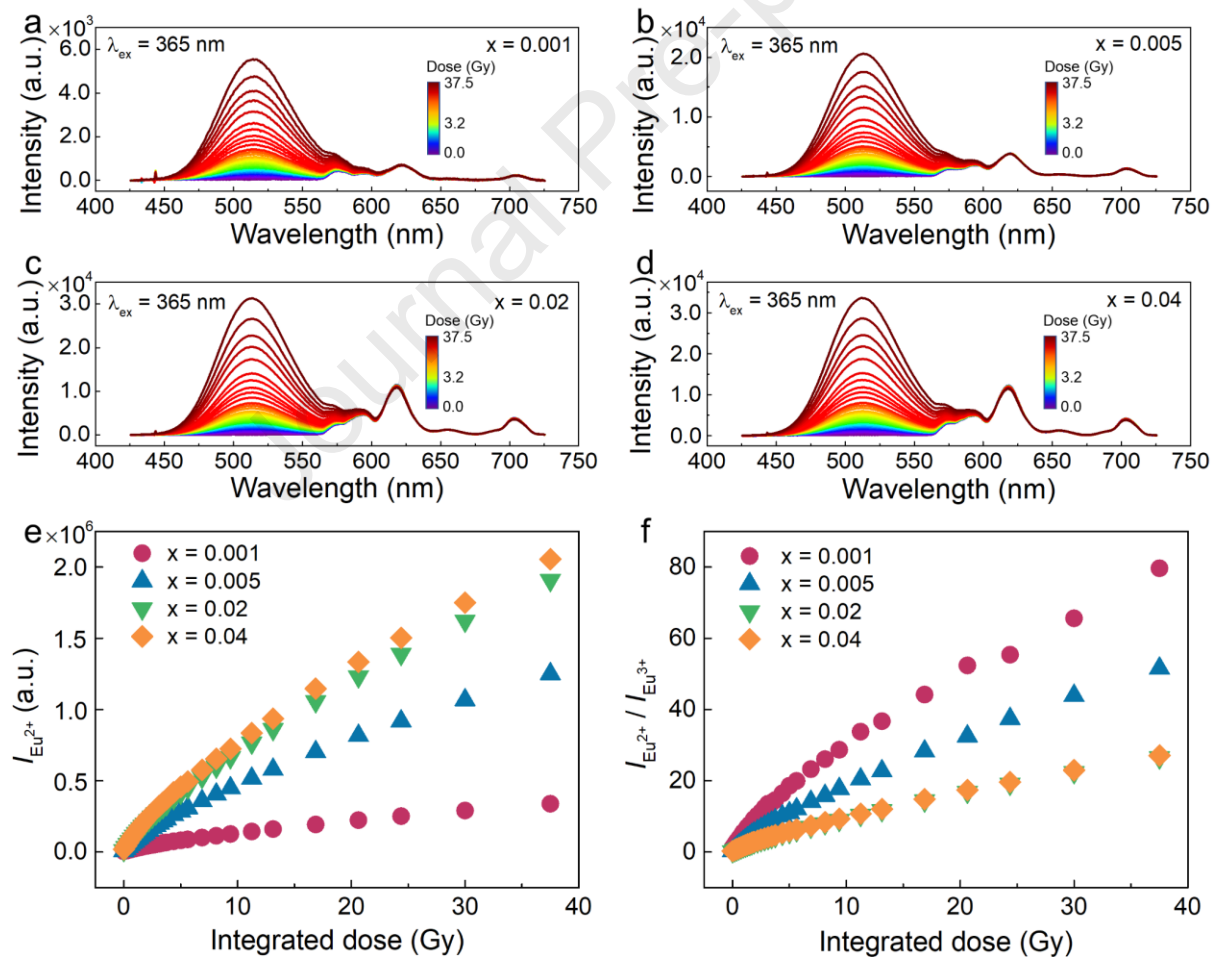


**Figure 2.** PL spectra ( $\lambda_{\text{ex}} = 365$  nm) of (a)  $\text{Ba}_{1.999}\text{Eu}_{0.001}\text{SiO}_4$ , (b)  $\text{Ba}_{1.995}\text{Eu}_{0.005}\text{SiO}_4$ , (c)  $\text{Ba}_{1.98}\text{Eu}_{0.02}\text{SiO}_4$  and (d)  $\text{Ba}_{1.968}\text{Eu}_{0.04}\text{SiO}_4$  after X-ray irradiation with different doses. Note that the color bars in the figures (a), (b), (c) and (d) are not linear. (e) Integrated PL intensity of

$\text{Eu}^{2+}$  ( $I_{\text{Eu}^{2+}}$ ) of  $\text{Ba}_{2-x}\text{Eu}_x\text{SiO}_4$  as a function of integrated doses. (f) Integrated PL intensity ratio between  $\text{Eu}^{2+}$  and  $\text{Eu}^{3+}$  ( $I_{\text{Eu}^{2+}}/I_{\text{Eu}^{3+}}$ ) of  $\text{Ba}_{2-x}\text{Eu}_x\text{SiO}_4$  as a function of integrated doses.

In previous research, the doping concentration dependency of the photoreduction behavior was ascribed to the partial luminescence quenching of created centers by surrounding defects.<sup>29,31</sup> To assess the plausibility of this explanation, the reflection spectra of  $\text{Ba}_{2-x}\text{Eu}_x\text{SiO}_4$  before and after irradiation with different doses were measured (Figure S2). The samples synthesized in air and in  $\text{N}_2+\text{H}_2$  are light green. The samples synthesized in air after X-ray irradiation are gray green. The reflectivity difference spectra (Figure 3a) show similar features, suggesting that the type of induced defects is similar for different doping concentrations. In addition, the photoluminescence decay curves of  $\text{Eu}^{2+}$  ( $4f^65d^1 \rightarrow 4f^7$  transition) in  $\text{Ba}_{2-x}\text{Eu}_x\text{SiO}_4$  synthesized in air after irradiation were recorded. All decay curves are well-fitted with a mono-exponential function (Figure 3b). The lifetime of photoinduced  $\text{Eu}^{2+}$  is comparable for different concentrations with a slight decrease as the concentration increases (Figure 3c). Furthermore, the lifetime of photoinduced  $\text{Eu}^{2+}$  is comparable to that of  $\text{Eu}^{2+}$  obtained by sintering in  $\text{N}_2+\text{H}_2$  (Figure S3). These results indicate that partial luminescence quenching of created  $\text{Eu}^{2+}$  is likely not the reason for the doping concentration dependency of photoreduction behavior in  $\text{Ba}_{2-x}\text{Eu}_x\text{SiO}_4$ .

EPR measurements were also performed to have an independent confirmation of the results obtained through luminescence spectroscopy. For each sample synthesized in air, the EPR spectrum was first recorded before irradiation and then measured again after irradiation with 450 Gy. As shown in Figure 3d and Figure S4, some signals related to impurities are observed in all samples before irradiation. These impurities are suspected to originate from the precursors, but it is difficult to confirm their chemical nature at this moment. After irradiation, other EPR signals appear, which can be attributed to  $\text{Eu}^{2+}$  ions through a comparison with the EPR spectrum of the sample sintered in  $\text{N}_2+\text{H}_2$ .<sup>14</sup> For the sample sintered in air, we conclude that most of the Eu ions are introduced in a trivalent since no EPR signal related to  $\text{Eu}^{2+}$  was observed. For the sample sintered in  $\text{N}_2+\text{H}_2$ , it is difficult to confirm that all of the Eu ions are incorporated into  $\text{Ba}_2\text{SiO}_4$  in their divalent state because the non-paramagnetic ion of  $\text{Eu}^{3+}$  does not produce EPR signals. In addition, for luminescent materials having an emission spectrum

dominated by emission originating from  $\text{Eu}^{2+}$  ions, a considerable fraction of  $\text{Eu}^{3+}$  ions can still be present in the sample.<sup>39,40</sup>

To better observe the signal of photoinduced  $\text{Eu}^{2+}$  ions, the EPR signals of the impurities were eliminated by taking the background of the unirradiated sample into account. This was done by subtracting the spectrum of the unirradiated sample divided by a factor  $>1$  that eliminates the features of the background spectrum in the wings (away from the central feature around 1200 mT). In this method, the central part of the spectrum gets distorted, but the largest wing features (marked in Figure 3e) used for estimating the relative concentrations have (in a good approximation) the same shape and position. The EPR signal difference spectra of  $\text{Ba}_{2-x}\text{Eu}_x\text{SiO}_4$  sintered in air after and before irradiation with 450 Gy are presented in Figure 3e. The result shows that the EPR signals related to  $\text{Eu}^{2+}$  ions increase as the doping concentration increases. Considering that the EPR signal intensity of  $\text{Eu}^{2+}$  is proportional to the number of  $\text{Eu}^{2+}$  ions, at the same irradiation dose a larger number of  $\text{Eu}^{2+}$  ions are produced as the doping concentration increases. However, one should notice that the number of photoreduced  $\text{Eu}^{2+}$  ions does not increase proportionally with the doping concentration. This indicates that X-rays induced conversion ratio of  $\text{Eu}^{3+}$  to  $\text{Eu}^{2+}$  tends to decrease as the doping concentration increases. If we assumed that all of the Eu ions are incorporated into  $\text{Ba}_2\text{SiO}_4$  in their divalent state for the lowest doping concentration ( $x = 0.001$ ) when synthesized in  $\text{N}_2+\text{H}_2$ , this sample can be selected as a reference to estimate the conversion ratio. By comparing the EPR signal intensity of photoreduced  $\text{Eu}^{2+}$  ions and of  $\text{Eu}^{2+}$  ions obtained by sintering in  $\text{N}_2+\text{H}_2$ , the conversion ratio of  $\text{Eu}^{3+}$  to  $\text{Eu}^{2+}$  was calculated to be 8%, 2.9%, 0.85% and 0.5% for  $x = 0.001, 0.005, 0.02$  and  $0.04$ , respectively, after irradiation at 450 Gy. The decreased conversion ratio leads to the observed concentration dependency of photoreduction behavior. In addition, the photoluminescence intensity of  $\text{Eu}^{2+}$  ( $I_{\text{Eu}^{2+}}$ ) is consistent with the number of created  $\text{Eu}^{2+}$  ions within uncertainties (Figure 3f). This further confirms that partial luminescence quenching of created  $\text{Eu}^{2+}$  is likely not the main mechanisms behind the concentration dependency of photoreduction behavior in  $\text{Ba}_{2-x}\text{Eu}_x\text{SiO}_4$ .

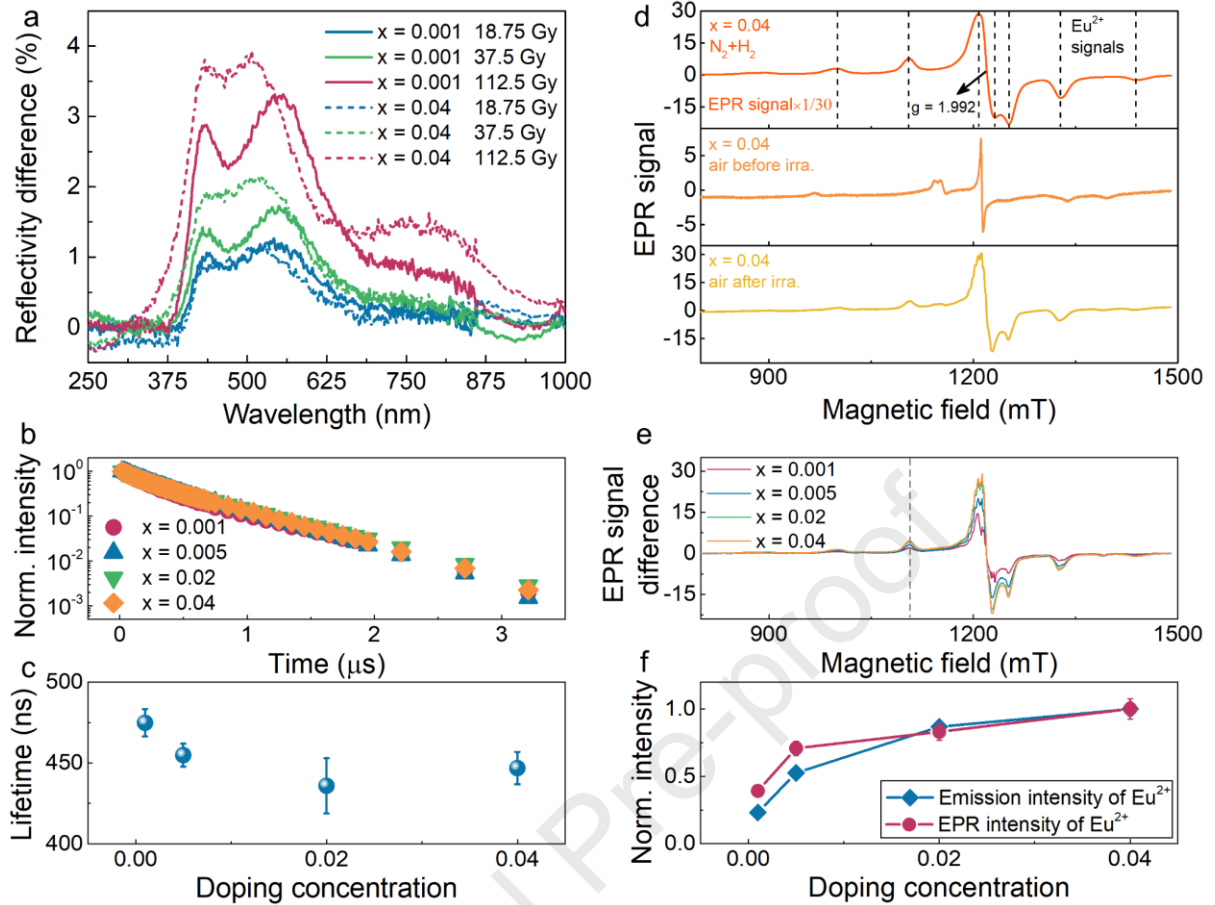


**Figure 3.** (a) Reflectivity difference of Ba<sub>1.999</sub>Eu<sub>0.001</sub>SiO<sub>4</sub> and Ba<sub>1.96</sub>Eu<sub>0.04</sub>SiO<sub>4</sub> after X-ray irradiation with different doses. (b) Decay curves ( $\lambda_{\text{ex}} = 415 \text{ nm}$ ) of Eu<sup>2+</sup> in Ba<sub>2-x</sub>Eu<sub>x</sub>SiO<sub>4</sub> synthesized in air after irradiation. (c) Lifetime of photoreduced Eu<sup>2+</sup> in Ba<sub>2-x</sub>Eu<sub>x</sub>SiO<sub>4</sub>. (d) EPR spectra of Ba<sub>1.96</sub>Eu<sub>0.04</sub>SiO<sub>4</sub> sintered in N<sub>2</sub>+H<sub>2</sub>, sintered in air before irradiation, and sintered in air after irradiation with 450 Gy. The dashed lines show the EPR signals of Eu<sup>2+</sup> ions. For a better comparison, the EPR signal of Ba<sub>1.96</sub>Eu<sub>0.04</sub>SiO<sub>4</sub> sintered in N<sub>2</sub>+H<sub>2</sub> is multiplied by 1/30. (e) EPR signal difference of Ba<sub>2-x</sub>Eu<sub>x</sub>SiO<sub>4</sub> after irradiation with 450 Gy. (f) A comparison of the emission intensity of Eu<sup>2+</sup> ( $I_{\text{Eu}^{2+}}$ ) and the EPR intensity of Eu<sup>2+</sup> ions in Ba<sub>2-x</sub>Eu<sub>x</sub>SiO<sub>4</sub> after 450 Gy irradiation.

To reveal the underlying mechanism for the decreased conversion ratio, optical spectroscopy experiments were performed. In previous research, it was shown that the Eu<sup>2+</sup> ions only occupy the 9-coordinated Ba sites (Ba2) when sintered in N<sub>2</sub>+H<sub>2</sub> based on the combination of density functional theory calculations and spectroscopy measurements,<sup>41</sup> while Eu<sup>3+</sup> ions can occupy multiple crystallographic sites when sintered in air<sup>42</sup>. This indicates that a site-dependent

preferential photoreduction process might exist in  $\text{Ba}_{2-x}\text{Eu}_x\text{SiO}_4$ . For  $\text{Eu}^{3+}$ , the non-degenerate  ${}^5D_0 \rightarrow {}^7F_0$  transition can be used to probe the presence of crystallographic inequivalent sites in a given host matrix.<sup>33,43</sup> The observation of three lines (Figure 4a, labeled as A, B and C) for the  ${}^5D_0 \rightarrow {}^7F_0$  transition reveals that  $\text{Eu}^{3+}$  ions occupy at least three crystallographic sites when synthesizing in air. Site-selective PLE spectroscopy (Figure 4b red, green and purple curves) reveals that all excitation spectra consist of a broad charge transfer (CT) band and a series of narrow lines originating from  $4f^6-4f^6$  transitions of  $\text{Eu}^{3+}$ , but the CT band of site A is located at a considerably lower energy in comparison with site B or site C. A comparison with the PLE spectrum of the same sample ( $\text{Ba}_{1.995}\text{Eu}_{0.005}\text{SiO}_4$ ) synthesized in air after irradiation with X-rays confirms that this abnormal broad band is related to the CT band of  $\text{Eu}^{3+}$  occupying site A instead of originating from transitions within  $\text{Eu}^{2+}$  present in the material as the excitation spectrum of the latter is much broader extending up to 450 nm. These observations are consistent with previous results where site A was postulated to correspond to  $\text{Eu}^{3+}$  ions located in an interstitial lattice site while site B and site C refer to  $\text{Eu}^{3+}$  ions replacing different  $\text{Ba}^{2+}$  sites.<sup>42</sup> A measurement of the luminescence lifetime (Figure 4c) shows that a much shorter luminescence lifetime (23  $\mu\text{s}$ ) of  $\text{Eu}^{3+}$  in site A is observed. This is compatible with the CT band of site A being at relatively long wavelengths as the CT band at low energies usually shorten the luminescence lifetime.<sup>33,44</sup> The decay curves of  $\text{Eu}^{3+}$  occupying site B and site C can be properly fitted with a double exponential function with a fast decay process (lifetime of around 30  $\mu\text{s}$ ) and a slow decay process. The decay time of  $\text{Eu}^{3+}$  in site B (lifetime of 1.24 ms) is longer than that of  $\text{Eu}^{3+}$  in site C (lifetime of 0.94 ms) (Figure 4c). In  $\text{Ba}_2\text{SiO}_4$ , the nine-fold oxygen coordination site (Ba2 site, mean Ba-O distance: 2.8205 Å) has a shorter mean Ba-O distance than that of the ten-fold oxygen coordination site (Ba1 site, mean Ba-O distance: 2.9946 Å).<sup>41</sup> A similar situation can be expected after substitution with  $\text{Eu}^{3+}$ . Typically, the position of the  ${}^5D_0 \rightarrow {}^7F_0$  transition for non-equivalent  $\text{Eu}^{3+}$  centers shifts toward longer wavelengths when Eu-O distances decrease.<sup>45</sup> It is therefore postulated that site B and site C correspond to  $\text{Eu}^{3+}$  ions occupying Ba1 sites and Ba2 sites, respectively. In addition, the occupancy situation of  $\text{Eu}^{3+}$  at different crystallographic sites depends on the doping concentration (Figure 4c). Since the relationship of the doping concentration and the PL intensity is still in the proportional regime (Figure 1e), it is reasonable to assume that the

luminescence intensity of  ${}^5D_0 \rightarrow {}^7F_0$  transition is proportional to the site population. In this case, it is inferred that the proportion of the Ba2 relative to Ba1 tends to decrease as the doping concentration increases.

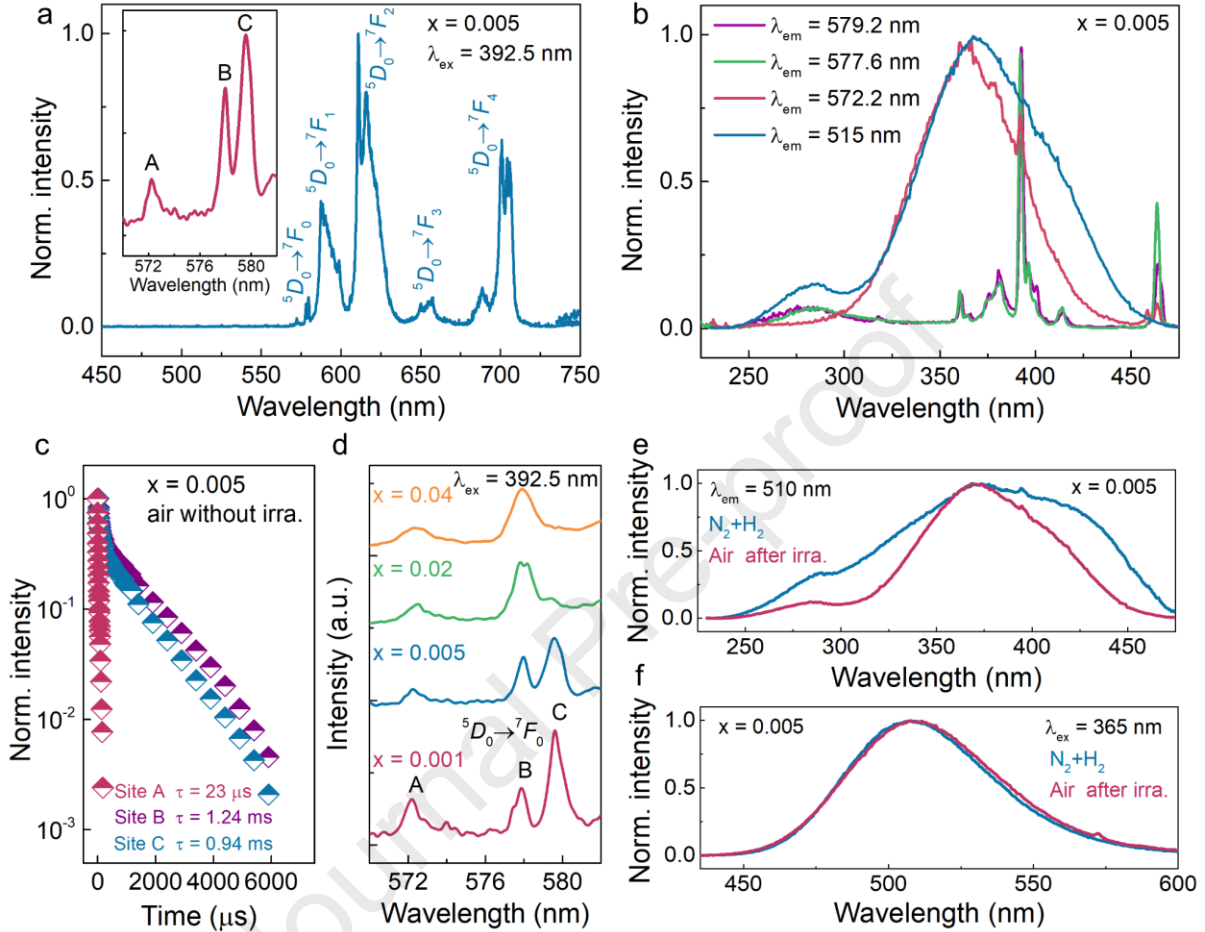


**Figure 4.** (a) Room-temperature PL spectra of  $\text{Ba}_{1.995}\text{Eu}_{0.005}\text{SiO}_4$  synthesized in air before irradiation; the inset shows the zoomed region of the  ${}^5D_0 \rightarrow {}^7F_0$  transition. (b) Room-temperature PLE spectra ( $\lambda_{\text{em}} = 572.2$  nm,  $577.6$  nm and  $579.2$  nm) of  $\text{Ba}_{1.995}\text{Eu}_{0.005}\text{SiO}_4$  before irradiation and PLE spectrum ( $\lambda_{\text{em}} = 515$  nm) of the same sample ( $\text{Ba}_{1.995}\text{Eu}_{0.005}\text{SiO}_4$ ) after X-ray irradiation. (c) Decay curves ( $\lambda_{\text{ex}} = 413$  nm) of  $\text{Eu}^{3+}$  at different crystallographic sites in  $\text{Ba}_{1.995}\text{Eu}_{0.005}\text{SiO}_4$  synthesized in air without X-ray irradiation. (d) PL spectra of the  ${}^5D_0 \rightarrow {}^7F_0$  transition of  $\text{Ba}_{2-x}\text{Eu}_x\text{SiO}_4$ . (e) Room-temperature PLE spectra of  $\text{Ba}_{1.995}\text{Eu}_{0.005}\text{SiO}_4$  sintered in  $\text{N}_2+\text{H}_2$  and sintered in air after X-ray irradiation. (f) Room-temperature PL spectra of  $\text{Ba}_{1.995}\text{Eu}_{0.005}\text{SiO}_4$  sintered in  $\text{N}_2+\text{H}_2$  and sintered in air after X-ray irradiation.

As shown in Figures 4e and 4f, the photoreduced sample shows similar PL and PLE

spectra of  $\text{Eu}^{2+}$  as the sample synthesized in  $\text{N}_2+\text{H}_2$ . The slight difference in the PLE spectra may be caused by the difference in the local environment around  $\text{Eu}^{2+}$  ions obtained by different methods. Furthermore, the PLE and PL spectra of either photoreduced samples or samples prepared in a reducing atmosphere are independent of the monitored emission wavelengths and used excitation wavelengths, respectively (Figure S5). These results indicate that the  $\text{Eu}^{2+}$  ions obtained by different methods (during synthesis or after photoreduction) occupy the same crystallographic site and these  $\text{Eu}^{2+}$  ions can only occupy one type of crystallographic site (Ba2) in  $\text{Ba}_2\text{SiO}_4$ . This is consistent with the results of lifetime measurements of  $\text{Eu}^{2+}$ , where a mono-exponential decay is observed for both the photoinduced  $\text{Eu}^{2+}$  and the reducing atmosphere-induced  $\text{Eu}^{2+}$ .

Based on the above results, we can conclude that the incorporated  $\text{Eu}^{3+}$  ions occupy at least three crystallographic sites in  $\text{Ba}_2\text{SiO}_4$  when synthesizing in air, while only  $\text{Eu}^{3+}$  ions occupying the Ba2 site can be photoreduced. Also, the occupation of  $\text{Eu}^{3+}$  ions at different crystallographic sites depends on the doping concentration. As the doping concentration increases, the proportion of  $\text{Eu}^{3+}$  on the site that can be photoreduced tends to decrease. The combination of these two effects may lead to the decreased conversion ratio of  $\text{Eu}^{3+} \rightarrow \text{Eu}^{2+}$  with increasing concentration at the same irradiation dose. However, some other factors such as the limited concentration of hole-trapping defects may also contribute to the concentration dependency of photoreduction behavior in  $\text{Ba}_{2-x}\text{Eu}_x\text{SiO}_4$  and further research is still required.

#### 4. Conclusion

In this work, we reported a doping concentration dependency of the photoreduction of  $\text{Eu}^{3+}$  in  $\text{Ba}_2\text{SiO}_4$  which shows great promise for medical imaging and ionizing radiation dosimetry. Systematic optical spectroscopy and electron paramagnetic resonance experiments are performed to reveal the underlying mechanisms. The results show that the incorporated  $\text{Eu}^{3+}$  ions occupy at least three crystallographic sites while only one type of  $\text{Eu}^{3+}$  site is photoreducible. As the doping concentration increases, the proportion of the crystallographic site that can be photoreduced relative to other sites tends to decrease. The combination of these two factors might induce the doping concentration dependency of conversion ratio, namely, a higher conversion ratio of  $\text{Eu}^{3+} \rightarrow \text{Eu}^{2+}$  is obtained under a low doping concentration after irradiation with the same dose. These findings provide insight into the photoinduced electron

transfer in luminescent materials and are beneficial for the development of high-performance dosimeters.

### Supporting Information

Supporting Information related to this article can be found in the online version.

### Acknowledgements

The authors acknowledge the financial support from the FWO (Fund for Scientific Research-Flanders, projects I002418N and G0F9322N).

### Conflict of Interest

The authors declare no conflict of interest.

### Data availability

The data that support the findings of this study are available from the corresponding author upon reasonable request.

### References

- 1 Feldmann, C., Jüstel, T., Ronda, C. R. & Schmidt, P. J. Inorganic luminescent materials: 100 years of research and application. *Adv. Funct. Mater.* **13**, 511-516, (2003).
- 2 Van der Heggen, D. *et al.* Persistent luminescence in strontium aluminate: A roadmap to a brighter future. *Adv. Funct. Mater.* **32**, 2208809, (2022).
- 3 Xu, J. & Tanabe, S. Persistent luminescence instead of phosphorescence: History, mechanism, and perspective. *J. Lumin.* **205**, 581-620, (2019).
- 4 Wu, J. *et al.* Dynamic readout of optical information based on the color-tunable emitting electron-trapping material BaAl<sub>12</sub>O<sub>19</sub>:Eu<sup>2+</sup> toward high security level optical data storage and anticounterfeiting. *Inorg. Chem. Front.* **10**, 2474-2483, (2023).
- 5 Van der Heggen, D., Joos, J. J. & Smet, P. F. Importance of evaluating the intensity dependency of the quantum efficiency: impact on LEDs and persistent phosphors. *ACS Photonics* **5**, 4529-4537, (2018).

- 6 Yuan, L. *et al.* Optically stimulated luminescence phosphors: Principles, applications, and prospects. *Laser Photonics Rev.* **14**, 2000123, (2020).
- 7 Yang, Z. T. *et al.* A versatile photochromic dosimeter enabling detection of X-ray, ultraviolet, and visible photons. *Laser Photonics Rev.* **17**, 2200809, (2023).
- 8 Zhang, Q. *et al.* Photoluminescence, thermoluminescence and reversible photoluminescence modulation of multifunctional optical materials Pr<sup>3+</sup> doped K<sub>x</sub>Na<sub>1-x</sub>NbO<sub>3</sub> ferroelectric ceramics. *J. Eur. Ceram. Soc.* **40**, 3946-3955, (2020).
- 9 Yang, Z., Hu, J., Martin, L. I. D. J., Van der Heggen, D. & Poelman, D. Realizing nondestructive luminescence readout in photochromic ceramics via deep ultraviolet excitation for optical information storage. *J. Mater. Chem. C* **9**, 14012-14020, (2021).
- 10 Joos, J. J., Van der Heggen, D., Amidani, L., Seijo, L. & Barandiarán, Z. Elucidation of the electron transfer mechanism in Eu<sup>2+</sup> and Sm<sup>3+</sup> codoped CaF<sub>2</sub>: A step towards better understanding of trapping and detrapping in luminescent materials. *Phys. Rev. B* **104**, L201108, (2021).
- 11 Joos, J. J., Neefjes, I., Seijo, L. & Barandiaran, Z. Charge transfer from Eu<sup>2+</sup> to trivalent lanthanide co-dopants: Systematic behavior across the series. *J. Chem. Phys.* **154**, 064704, (2021).
- 12 Kong, J. & Meijerink, A. Identification and quantification of charge transfer in CaAl<sub>2</sub>O<sub>4</sub>:Eu<sup>2+</sup>,Nd<sup>3+</sup> persistent phosphor. *Adv. Optical Mater.*, 2203004, (2023).
- 13 Joos, J. J. *et al.* Identification of Dy<sup>3+</sup>/Dy<sup>2+</sup> as electron trap in persistent phosphors. *Phys. Rev. Lett.* **125**, 033001, (2020).
- 14 Yang, Z. *et al.* Realizing simultaneous X-ray imaging and dosimetry using phosphor-based detectors with high memory stability and convenient readout process. *Adv. Funct. Mater.* **32**, 2201684, (2022).
- 15 Volhard, M.-F. & Jüstel, T. The effect of X-ray exposure on Ba<sub>2</sub>SiO<sub>4</sub>:Eu<sup>3+</sup>. *Opt. Commun.* **410**, 617-622, (2018).
- 16 Yukihiro, E. G. *et al.* Luminescence dosimetry. *Nat. Rev. Methods Primers* **2**, 26, (2022).
- 17 Yanagida, T., Okada, G. & Kawaguchi, N. Ionizing-radiation-induced storage-luminescence for dosimetric applications. *J. Lumin.* **207**, 14-21, (2019).
- 18 Iwao, M. *et al.* Ag-doped phosphate glass with high weathering resistance for RPL

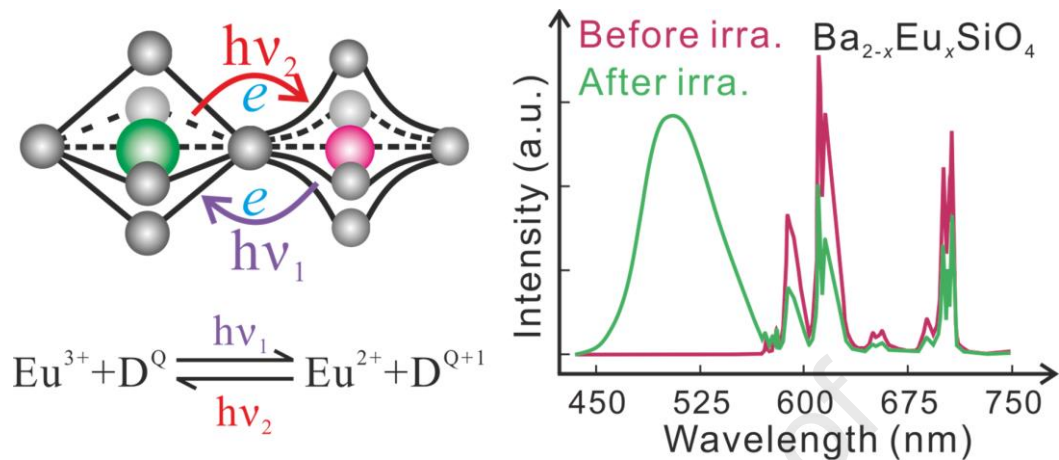
- dosimeter. *Radiat. Meas.* **140**, 106492, (2021).
- 19 McKeever, S. W. S., Sholom, S., Shrestha, N. & Klein, D. M. Build-up of radiophotoluminescence (RPL) in Ag-doped phosphate glass in real-time both during and after exposure to ionizing radiation: A proposed model. *Radiat. Meas.* **132**, 106246, (2020).
- 20 Akselrod, M. S. & Akselrod, A. E. New Al<sub>2</sub>O<sub>3</sub>:C,Mg crystals for radiophotoluminescent dosimetry and optical imaging. *Radiat. Prot. Dosim.* **119**, 218-221, (2006).
- 21 Tsuta, M., Nakamura, S. & Kato, A. Effect of laser fluence and charge compensation defects on photoreduction of Eu ions in K<sub>2</sub>SrPO<sub>4</sub> crystal using a UV laser. *J. Lumin.* **244**, 118755, (2022).
- 22 Fujimoto, Y. *et al.* Radiation induced change in the optical properties of NaCl:Yb crystal. *Radiat. Meas.* **133**, 106274, (2020).
- 23 Okada, G. *et al.* Samarium-doped oxyfluoride glass-ceramic as a new fast erasable dosimetric detector material for microbeam radiation cancer therapy applications at the canadian synchrotron. *J. Am. Ceram. Soc.* **97**, 2147-2153, (2014).
- 24 Calvert, R. L. & Danby, R. J. Thermoluminescence and radiophotoluminescence from Eu- and Sm-doped CaSO<sub>4</sub>. *phys. stat. sol.* **88**, 597-604, (1984).
- 25 Hu, J. *et al.* To luminesce or to change valence? Insight into the wavelength dependency of the reversible valence switching of europium in Sr<sub>3</sub>SiO<sub>5</sub>. *J. Phys. Chem. C* **126**, 21396-21404, (2022).
- 26 Okada, G. *et al.* Spatially resolved measurement of high doses in microbeam radiation therapy using samarium doped fluorophosphate glasses. *Appl. Phys. Lett.* **99**, 121105, (2011).
- 27 Riesen, N., Francois, A., Badek, K., Monro, T. M. & Riesen, H. Photoreduction of Sm<sup>3+</sup> in nanocrystalline BaFCl. *J. Phys. Chem. A* **119**, 6252-6256, (2015).
- 28 Okada, G., Kawaguchi, N., Kasap, S., Nanto, H. & Yanagida, T. Radiophotoluminescence properties of LiCaAlF<sub>6</sub>:Sm. *Radiat. Meas.* **132**, 106251, (2020).
- 29 Morrell, B. *et al.* Optically erasable samarium-doped fluorophosphate glasses for high-dose measurements in microbeam radiation therapy. *J. Appl. Phys.* **115**, 063107, (2014).
- 30 Okada, G. *et al.* X-ray induced reduction of Sm<sup>3+</sup> into Sm<sup>2+</sup> in Li<sub>2</sub>CaSiO<sub>4</sub> and its

- potential for radiation measurement applications. *Mater. Res. Bull.* **159**, 112107, (2023).
- 31 Okada, G., Shinozaki, K., Shiratori, D., Kawaguchi, N. & Yanagida, T. Radiophotoluminescence observed in Eu-doped BABF glass-ceramics. *Ceram. Int.* **45**, 9376-9380, (2019).
- 32 Lin, L. *et al.* Luminescence properties and site occupancy of Ce<sup>3+</sup> in Ba<sub>2</sub>SiO<sub>4</sub>: a combined experimental and ab initio study. *RSC Adv.* **7**, 25685-25693, (2017).
- 33 Binnemans, K. Interpretation of europium(III) spectra. *Coord. Chem. Rev.* **295**, 1-45, (2015).
- 34 Joos, J. J., Smet, P. F., Seijo, L. & Barandiarán, Z. Insights into the complexity of the excited states of Eu-doped luminescent materials. *Inorg. Chem. Front.* **7**, 871-888, (2020).
- 35 Zhang, M., Wang, J., Zhang, Q., Ding, W. & Su, Q. Optical properties of Ba<sub>2</sub>SiO<sub>4</sub>:Eu<sup>2+</sup> phosphor for green light-emitting diode (LED). *Mater. Res. Bull.* **42**, 33-39, (2007).
- 36 Bispo, A. G., Ceccato, D. A., Lima, S. A. M. & Pires, A. M. Red phosphor based on Eu<sup>3+</sup>-isoelectronically doped Ba<sub>2</sub>SiO<sub>4</sub> obtained via sol-gel route for solid state lightning. *RSC Adv.* **7**, 53752-53762, (2017).
- 37 Yanagida, T., Okada, G., Kato, T., Nakauchi, D. & Kawaguchi, N. A review and future of RPL dosimetry. *Radiat. Meas.* **158**, 106847, (2022).
- 38 Yang, Z. *et al.* Personal solar UV monitoring based on photoinduced electron transfers in luminescent materials. *Adv. Optical Mater.*, 2023, DOI: 10.1002/adom.202300733.
- 39 Li, S. *et al.* Achieving high quantum efficiency narrow-band  $\beta$ -sialon:Eu<sup>2+</sup> phosphors for high-brightness LCD backlights by reducing the Eu<sup>3+</sup> luminescence killer. *Chem. Mater.* **30**, 494-505, (2017).
- 40 Avci, N., Korthout, K., Newton, M. A., Smet, P. F. & Poelman, D. Valence states of europium in CaAl<sub>2</sub>O<sub>4</sub>:Eu phosphors. *Opt. Mater. Express* **2**, 321-330, (2012).
- 41 Lin, L. *et al.* Site occupation of Eu<sup>2+</sup> in Ba<sub>2-x</sub>Sr<sub>x</sub>SiO<sub>4</sub> (x = 0-1.9) and origin of improved luminescence thermal stability in the intermediate composition. *Inorg. Chem.* **57**, 7090-7096, (2018).
- 42 Pires, A. M., Davolos, M. R. & Malta, O. L. Eu<sup>3+</sup>-O<sup>2-</sup> associates luminescence in Ba<sub>2</sub>SiO<sub>4</sub>. *J. Lumin.* **72-74**, 244-246, (1997).

- 43 Tanner, P. A. Some misconceptions concerning the electronic spectra of tri-positive europium and cerium. *Chem. Soc. Rev.* **42**, 5090-5101, (2013).
- 44 Hoshina, T., Imanaga, S. & Yokono, S. Charge transfer effects on the luminescent properties of  $\text{Eu}^{3+}$  in oxysulfides. *J. Lumin.* **15**, 455-471, (1977).
- 45 Benhamou, R. A. *et al.* New insight in the structure–luminescence relationships of  $\text{Ca}_9\text{Eu}(\text{PO}_4)_7$ . *J. Solid. State. Chem.* **182**, 2319-2325, (2009).

Journal Pre-proof

## Graphical abstract



The concentration dependency of the photoreduction of  $\text{Eu}^{3+}$  in  $\text{Ba}_2\text{SiO}_4$  was revealed based on the combination of optical spectroscopy and electron paramagnetic resonance measurements. This functional behavior can be employed for medical imaging, ionizing radiation dosimetry and anti-counterfeiting applications.

1. Photoinduced reversible valence change of  $\text{Eu}^{3+} \leftrightarrow \text{Eu}^{2+}$  was achieved in  $\text{Ba}_{2-x}\text{Eu}_x\text{SiO}_4$  ceramics accompanied by a significant change in photoluminescence color, which can be employed for medical imaging, ionizing radiation dosimetry and anti-counterfeiting applications.
2. The concentration dependency of the photoreduction of  $\text{Eu}^{3+}$  in  $\text{Ba}_2\text{SiO}_4$  ceramics was revealed due to the combined factors of site-dependent photoreduction and concentration-dependent occupancy situation of  $\text{Eu}^{3+}$  at different crystallographic sites.
3. This work provides much-needed insights into the photoinduced electron transfer in luminescent materials and can facilitate the exploration of this functional behavior for advanced devices.

### **Author contributions**

**Zetian Yang:** conceptualization, methodology, formal analysis, investigation, writing original draft

**Jieqi Hu:** writing – review & editing, methodology

**David Van der Heggen:** writing – review & editing, methodology

**Mengmeng Jiao:** writing – review & editing, methodology

**Henk Vrielinck:** formal analysis, investigation writing – review & editing, investigation

**Philippe F. Smet:** conceptualization, writing – review & editing, supervision

**Dirk Poelman:** conceptualization, resources, writing – review & editing, supervision, project administration

**Declaration of interests**

The authors declare that they have no known competing financial interests or personal relationships that could have appeared to influence the work reported in this paper.

The authors declare the following financial interests/personal relationships which may be considered as potential competing interests:

Journal Pre-proof